https://doi.org/10.5194/egusphere-2025-2746
Preprint. Discussion started: 28 July 2025

Linear trends of temperature, salinity, and oxygen in the North Pacific based on GOBAI-O_2 over 2 decades and their controlling factors

Miho Ishizu[1, 2], Tomomichi Ogata[3]

[1]*Center for Climate Physics, Institute for Basic Science, Busan 46241, Republic of Korea*
[2]*Pusan National University, Tonghapgigyegwan Bldg 2 Busandaehak-ro, 63 beon-gil, Geumjeong-gu, Busan 46241, Republic of Korea*
[3]*Japan Agency for Marine-Earth Science and Technology, Environmental Variability Prediction and Application Research Group, Yokohama Institute for Earth Sciences, 3173-25 Showa-machi, Kanagawa-ku, Yokohama 236-0001, Japan*
To whom correspondence may be addressed. Email: mishizu@pusan.ac.kr

Abstract

Oxygen concentrations in the ocean are believed to be declining due to global warming. However, our understanding of its variability remains limited compared to physical parameters such as temperature and salinity, because oxygen is difficult to observe with high spatial and temporal resolution. In this study, we analyzed linear trends in potential temperature, salinity, and dissolved oxygen in the North Pacific over the past two decades (2004–2023), using the GOBAI-O_2 data. We then compared oxygen trends with physical parameters to investigate the spatial pattern of linear changes across the region. The oxygen trends derived from GOBAI-O_2 were consistent with those observed along hydrographic lines that have been relatively frequently and continuously surveyed by ship-based observations. Although an overall declining trend in dissolved oxygen was evident, localized increases were observed in certain density layers. By examining the associated physical conditions, we found that the spatial heterogeneity of the oxygen trends can be attributed to known oceanographic processes, such as the southward retreat of the oxygen minimum layer and the northward migration of a recently

https://doi.org/10.5194/egusphere-2025-2746
Preprint. Discussion started: 28 July 2025

identified front separating the subtropical and subarctic gyres. Our findings highlight the utility of GOBAI-O_2 data in linking physical changes to previously unrecognized biological and biogeochemical patterns in the ocean.

Plain Language Summary

1. We examined the linear trends in potential water temperature, salinity, and dissolved oxygen in North Pacific over the past 20 years using GOBAI-O_2 data and explored the mechanisms behind these trends.
2. Our findings confirmed that the observed trends are confirmed to be consistent with findings from previous studies, and further reveal spatial trend linkages that had only been partially recognized.
3. The results showed an overall decreasing trends, but in some localized areas, an increasing trend was observed, indicating the fluctuations were not ununiform. The reason for the non-uniformity is related to well-known physical phenomena such as the south retreat of oxygen minimum layer in the North Pacific and a recently discovered change in the meridional shift of the front between the subtropical and subarctic gyres toward the north.
4. The result of this study provides one of the pieces of evidence linking physical changes to previously unclear changes in biological observations.

Keywords: dissolved oxygen, 20-year linear trends, Bio-Argo float data, global warming

1. Introduction

Recent decades have witnessed a reduction in the global ocean's dissolved oxygen inventory, a trend that is projected to continue over the course of the 21th century [Keeling et al., 2010; Breitburg et al., 2018; Stramma and Schmidtko, 2021; Limburg et al., 2020]. This decline is attributed to the release of oxygen from the ocean due to oxygen solubility resulting from rising surface temperatures.

https://doi.org/10.5194/egusphere-2025-2746
Preprint. Discussion started: 28 July 2025

Additionally, enhanced stratification and stagnation of ocean circulation caused by global warming are also contributing factors [Keeling et al., 2010, Bopp et al. 2013; Ito et al. 2017]. Oxygen outgassing can have harmful effects on aerobic marine organisms [Pörtner and Farrell, 2008; Sampaio et al., 2021] and may alter biogeochemical cycles and trigger important climatological feedback [Berman-Frank et al., 2008]. Historical deoxygenation has been inferred from analyses of globally distributed observation data [Helm et al., 2011; Schmidtko et al., 2017; Ito et al., 2017; Takatani et al., 2012; Sasano et al., 2014; Lauvset et al., 2022b]. Earth system models have been used to simulate historical and projected future deoxygenations of the oceans [Bopp et al., 2013; Frolicher et al., 2009; Kwiatkowski et al., 2020; Li et al. 2020].

Oxygen trends have been observed and discussed using the discrete measurements of dissolved oxygen concentration (O_2). These measurements are usually made by Winker titration [Winkler, 1988; Carpner, 1965]. These titrations are also used to calibrate the readings of electrode (or more recently optical) dissolved oxygen sensors attached to conductivity-water temperature-depth (CTD) profilers [Helme et al. 2011; Schmidtko et al., 2017; Ito et al., 2017; Lauvset et al., 2022b]. However, WOCE, CLIVAR, and GO-SHIP have a 10-year unit time resolution, which does not allow for a robust analysis of annual or seasonal variations in O_2. Some O_2 data are relatively frequently observed in a specific local area during a year [Takatani et al. 2012, Sasano et al., 2014], but they are localized, and so it is difficult to know how the phenomena are connected or disconnected each other, although some research did the trials to understand the spatial variability of oxygen [Strammer et al. 2020]. Therefore we must have a very limited spatial-temporal understanding of the observed data in dissolved oxygen.

Oxygen sensors were first installed on Argo profiling floats in the mid-2000s, and since then, approximately 1,800 of these floats, equipped with oxygen sensors, have been deployed in ocean around the world, advancing efforts to deepen our understanding of trends and variability in oceanic oxygen levels [Sharp et al., 2023]. The effort to establish a global biogeochemical Argo network has led to the deployment of oxygen-sensor-equipped Argo floats in regions of the ocean that were previously less sampled [Claustre et al., 2020]. As the number of deployed floats has grown, significant

https://doi.org/10.5194/egusphere-2025-2746
Preprint. Discussion started: 28 July 2025

progress has been made in sensor calibration, data adjustments, and quality control. Noteworthy improvements include pre-deployment drift corrections [D'Asaro and McNeil, 2013; Johnson et al., 2015; Bitting and Kortzinger, 2015; Bushinsky et al., 2016; Drucker and Riser, 2016; Nicholson and Feen, 2017], climatology-based calibrations [Takeshita et al., 2013], in-air oxygen measurement calibrations [Kortzinger et al., 2005; Fiedler et al., 2013; Bitting and Kortzinger, 2015; Johnson et al., 2015; Bushinsky et al., 2016], post-deployment drift corrections [Johnson et al., 2017; Bitting et al., 2018a], and the development of procedures for delayed-mode quality control [Maurer et al., 2021]. These advancements have significantly reduced measurement uncertainty and improved the consistency of optode-based [O_2] measurements from Argo floats.

Measurement data from oxygen sensors installed on the Argo float have primarily been used for localized process studies. Specially, these studies have focused on air-sea oxygen exchange [Wolf et al., 2018], upper-ocean primary production [Alkire et al., 2012; Estapa et al., 2019], the efficiency of the biological pump [Johnson and Bif, 2021], and the dynamics of oxygen minimum zone [Udaya Bhaskar et al., 2021]. However, Sharp et al. [2023] recently produced a four-dimensional gridded [O_2] product, called GOBAI-O_2 (Gridded Ocean Biogeochemistry from Artificial Intelligence – Oxygen) [Sharp et al., 2022; https://doi.org/10.25921/z72m-yz67]. GOBAI-O_2 is developed using machine learning (ML), a subfield of AI that specializes in training, understanding, and applying algorithms that learn and reproduce patterns artificially using data. Their analysis demonstrates that the GOBAI-O_2 data can reveal spatial patterns, seasonal cycles, and decadal variability, with particular emphasis on the potential for these data to serve as valuable new observational assets in areas where observational data gaps and high background O_2 variablity overlap.

Regarding the oxygen trends in the North Pacific, Ito et al. [2017] used the objectively mapped monthly climatology of O_2 based on the World Ocean Database 2013 (WOD13) [Boyer et al., 2013] at standard depths from 1958 to 2015 and found multidecadal trends and variability in dissolved oxygen in the surface layer. Sasano et al. [2014] detected significant warming trends and circulation changes by using the JMA's high-frequency shipboard observational sections along the 137°E and

https://doi.org/10.5194/egusphere-2025-2746
Preprint. Discussion started: 28 July 2025

165°E lines from 1987 to 2011 in the western North Pacific. Their results showed that the O_2 declines in the northern subtropical to subtropical-subarctic transition zones averaged -0.45 ± 0.16 μmol/kg/yr at 25.3 σ_θ and -0.45 ± 0.14 μmol/kg/yr at 26.8 σ_θ, respectively. Significant increasing trends in O_2 were detected in the tropical Oxygen Minimum Layer (OML), with an increase of +0.36 ± 0.004 μmol/kg/yr. Their analysis revealed the spatial heterogeneity in the observed O_2 trends. Significant and extensive O_2 declines were observed in the subpolar North Pacific and off the California coast, while modest O_2 increase occurred in the mid-subtropical and western tropical North Pacific.

For horizontal broad-scale trends in the North Pacific, Strammer et al. [2020] analyzed horizontal data using data from the Hydro base and the World Ocean Database bottle, and found linear trends and the Pacific Decadal Oscillation (PDO) in the tropical and eastern Pacific Ocean, In particular, they found that climate signals such as the North Pacific Gyre Oscillation (NPGO) in the North Pacific, and the 18.6-year oscillation at depths between 50 and 300 m in the equatorial and North Pacific are found, as are physical fields such as water temperature and salinity. Although they collected as much data as possible and analyzed them separately by region, it was difficult to ascertain the physical significance of how these data trends are connected or not.

Opportunities to understand specific trends in dissolved oxygen, including those associated with trends in ocean temperature and salinity, are currently limited and will remain so in the future due to constrained observational resources. Data such as those from GOBAI-O_2 will therefore become increasingly valuable for understanding trends at basin scales. Understanding how dissolved oxygen is changing is also crucial for assessing the impact on marine organisms [Breitburg et al. 2018]. Argo floats equipped with oxygen sensors will continue to be deployed in the future. In this study, we present the linear trends of temperature, salinity, and oxygen using the GOBAI-O_2 data set from 2004 to 2023 in the North Pacific, and how their trends connect each other. In the discussion section, we show how oxygen changes are influenced by factors such as global warming and the physical oceanic background in the North Pacific.

https://doi.org/10.5194/egusphere-2025-2746
Preprint. Discussion started: 28 July 2025

2. Data and processing

The four-dimensional gridded product (GOBAI-O_2) data in ocean interior oxygen are generated using machine learning algorithms trained on dissolved oxygen data from Argo float sensors and ship-based discrete observations. These data are applied to temperature and salinity distributions constructed from the global Argo array (Roemmich and Gilson, 2009). The GOBAI-O_2 data originate from the combined datasets of ship-based surveys (GLODAP version 2022) and Argo float data (Argo Global Data Assembly Centres), which are processed after quality control [Sharp et al., 2022, 2023] (https://doi.org/10.25921/z72m-yz67). The combined dataset served as training input for machine learning algorithms to predict [O_2], based on variables such as absolute salinity, conservative temperature, potential density anomaly, hydrostatic pressure, bottom depth, and additional spatiotemporal information representing geographic, seasonal, and interannual variability. While biological processes are not directly incorporated into the machine learning algorithms, Giglio et al. [2018] showed how incorporating spatiotemporal variables can effectively capture their influence implicitly for biological processes.

The development of GOBAI-O_2 involved the use of these two types of machine learning algorithms—random forest regressions and feed-forward neural networks: feed-forward neural networks (FNNs) and random forest regressions (RFRs) [Breiman, 2001]. The average of the FNN and RFR estimates was used as the [O_2] estimate for a given input data point. The data cover 86% of the global ocean area on a 1° × 1° (latitude × longitude) grid, spanning the years 2004–2023 with a monthly resolution. The vertical levels range from the ocean surface to a depth of 2 km, with 58 levels. Sharp et al. [2023] evaluated 0.79 ± 0.04% per decade decrease in the oxygen inventory of the upper 2 km of the global ocean over the period 2004–2022. More details of their data sources, processing, algorithm training, evaluation, and uncertainty estimation are provided in Sharp et al. [2023].

In our analysis, we gridded the data to a 1° × 1° × 1 m grid using vertical cubic spline interpolation from the original GOBAI-O_2 and Roemmich and Gilson (2009) data [Figs. 1, 2]. Linear trends in

https://doi.org/10.5194/egusphere-2025-2746
Preprint. Discussion started: 28 July 2025

potential temperature, salinity, and dissolved O_2 changes were calculated at each depth, as shown in Figs. 1 and 2, and for each latitudinal band at 1° intervals in latitude and at $0.1\sigma_\theta$ intervals in Fig. 3. We selected isopycnal horizon data at 25.0, 26.0, and 26.8 σ_θ and calculated the linear trends for each horizontal surface [Figs. 4 and 6]. The uncertainty estimates (Figure S1) and the coefficient of determination of the linear regression line (Figure S2) on the 25.0, 26.0, and 26.8 σ_θ isopycnal surfaces are shown in the supplemental materials.

3. Results

3.1 Horizontal distributions of linear trends

Figures 1 show the horizontal and vertical distributions of linear trends in potential temperature, salinity, and dissolved oxygen from 2004 to 2024. Positive trends in potential temperature are primarily distributed in the surface layer above 200 m depth (Fig. 1a–c). Trends are relatively strong in the higher latitudes. Negative trends appeared below the surface from the eastern tropical area (180°–120°W, 5°–15°N) (Fig. 1b). This area extends westward and deepens with increasing depth (Fig. 1d–f). Positive and negative trends are distributed differently in the subarctic and subtropical gyres below 400 m depth.

Negative trends in salinity are generally observed throughout the surface layer (Fig. 1h–i), with localized positive trends in the Kuroshio–Oyashio transition area and the northwest Pacific (140°–180°E, 20°–50°N), as well as in the tropical region (120°–170°E, 0°–10°N). Some positive trends are also detected in the eastern California coastal area (130°–199°W, 20°–40°N). Below 200 m depth, weak positive and negative trends are evident, mirroring the trends in potential temperature (Fig. 1j–k). Positive and negative trends tend to be distributed differently in the subarctic and subtropical gyres. The negative trends are detected around the Alaska gyre (170°–130°W, 40°–55°N) (Fig. 1j-l), which differs from the distribution of potential temperature.

Negative trends in dissolved oxygen are distributed both horizontally and zonally throughout the

https://doi.org/10.5194/egusphere-2025-2746
Preprint. Discussion started: 28 July 2025

depth range (Fig. 1o–u). Large negative trends are observed in the high latitudes and weaker with latitude near the surface. The location of these trends shifts with depth. Notably, large negative trends occur along the northeast coastal region (140°–130°W, 40°–50°N) and the southern region (10°–25°N) within the density range of 25.2–26.8σ_θ, from 200 to 600 m depth (Fig. 1q–s). Weak positive trends are partially detected around the Kuroshio–Oyashio transition area (130°–150°E, 30°–40°N) below 200 m depth. These positive trends extend into deeper layers and spread northeastward across the North Pacific (Fig. 1r–u). Positive trends are only observed in specific regions: the tropical region at 100 m depth (Fig. 1p); the Alaska Gyre at 200–400 m depth (Fig. 1q–r); the western tropical region at 400–600 m depth (Fig. 1r–s); and the Kuroshio–Oyashio transition region at 400–600 m depth (Fig. 1r–s).

3.2 Vertical sections and isopyncal density analysis of liner trends in 137°E and 165°E lines

We picked up the vertical sections and isopycnal density distributions of linear trends in potential temperature, salinity, and dissolved oxygen along the 137°E and 165°E lines to compare with historical observational results reported by Ogata and Nonaka [2020] and Sasano et al. [2014] (Fig. 2). (Ogata and Nonaka [2020] used temperature and salinity data from 40 years of cruises along the 137°E line between 1967 and 2009, while Sasano et al. [2014] analyzed temperature, salinity, and dissolved oxygen data from 25 years of cruises along the 165°E line between 1987 and 2011.) Large negative trends in temperature and salinity were detected along the 25.0–26.0σ_θ isopycnal, corresponding to a potential temperature of 10–12°C and salinity of 34.4–34.5. In contrast, large negative trends in dissolved oxygen were observed along the 26.0–27.0σ_θ isopycnal, indicating that the areas showing significant trends in dissolved oxygen differ from those of temperature and salinity. Additionally, large positive trends in dissolved oxygen were observed south of 15°N below 200 m depth along the 137°E line (Fig. 2c), corresponding to the upper boundary of the OML.

The distributions of trends in temperature and salinity on the isopycnal horizons show distinct

https://doi.org/10.5194/egusphere-2025-2746
Preprint. Discussion started: 28 July 2025

differences for temperature, and salinity and dissolved oxygen (Fig. 3). The linear trends in temperature and salinity are closely aligned, indicating that warming occurs with increasing salinity, while cooling occurs with decreasing salinity (Fig. 3a–b, d–e). Distinct positive trends in temperature and salinity are observed in the density range of 22.0–26.0σ_θ in the tropical region (5°S–5°N). No noticeable trends are found in the salinity minimum region (S = 34–34.1) within the density range of 26.5–27.0σ_θ. At higher latitudes (40°–50°N), large positive trends are evident in the density range of 26.0–27.0σ_θ (Fig. 3e). For dissolved oxygen, negative trends dominate overall; however, weak positive trends are observed throughout the density range of 23.0–26.0σ_θ in low-latitude regions (5°S–5°N). Additionally, large positive trends are present in the deeper density range of 26.0–27.0σ_θ in the 5°–10°N band. Weak positive trends are also detected between 10°–20°N in the density range of 23.0–25.0σ_θ along both the 137°E and 165°E lines.

The temperature and salinity of GOBAI-O_2 data [Roemmich and Gilson, 2009; Sharp et al., 2023] reveals a much wider area with negative trends in salinity in the density range of 22.0–24.0σ_θ along the 137°E line compared to the results reported by Ogata and Nonaka [2020]. The general characteristics of the linear trends in potential temperature and salinity align closely with the findings of Sasano et al. [2014], although the current results are notably smoother, particularly for dissolved oxygen. This smooth distribution may be due in large part to the smoothing process applied to the data. The shipboard observations by Sasano et al. [2014] identified patchy positive trends in oxygen within the density range of 24.5–27.5σ_θ in the regions of 5°–15°N and 6°S–1°N. In contrast, the current data depicts a broader, smoother, and more consistent positive trend spreading in the tropical region (-6°S–5°N). The repeated shipboard observations also identified localized positive trends in deeper layers within the density range of 26.5–27.5σ_θ. However, the current data more clearly highlights the core of negative trends in oxygen within 5°–15°N (Fig. 3c and f). These trends represent the negative signals extending along the lower isopycnals, which are characteristic of the subtropical gyre.

https://doi.org/10.5194/egusphere-2025-2746
Preprint. Discussion started: 28 July 2025

3.3 Horizontal distribution of linear trends along isopycnal surfaces

3.3.1 Potential temperature and salinity

The horizontal distributions of linear trends in potential temperature, salinity, and dissolved oxygen on specific isopycnal surfaces at 25.0, 26.0, and 26.8σ_θ (Fig. 4) are illustrated to explore how these trends occur and connect each other. These density surfaces correspond to the shallower densities of Subtropical Mode Water (STMW), the shallower densities of Central Mode Water (CMW) [Suga et al., 1997; 2004], and the representative density of North Pacific Intermediate Water (NPIW) [Nakamura et al., 2000a, b; Nakamura and Awaji, 2004; Yasuda, 2004], respectively. STMW is formed south of the Kuroshio Extension, between 30–35°N and 130–170°E, and penetrates to depths of about 400 m in late winter. It then spreads nearly to the subtropical front through advection across the Kuroshio recirculation area. CMW is formed in the transition area of the central North Pacific and spreads eastward along the North Pacific Current before turning southward and westward in the subtropical gyre [Suga et al., 1997; 2004]. In contrast, NPIW does not outcrop during its formation process in the North Pacific. Its origin lies in Okhotsk Sea Mode Water, which is formed through overturning driven by diapycnal upwelling and tidal mixing around the Kuril Islands [Nakamura et al., 2000a, b; Nakamura and Awaji, 2003; You, 2003; Yasuda, 2004; Yasuda, 2004] as well as double diffusions in the North Pacific [You, 2003].

The distributions of linear trends on the 25.0, 26.0, and 26.8σ_θ isopycnal surfaces indicate that positive and negative trends are linked to specific locations. These trends are generally distributed according to the geostrophic streamlines (Fig. 4a–b, d–e, g–h). Although there are exceptions, such as the region showing weak positive (150–175°E, 20–30°N) (Fig. 4a–b), negative trends in temperature and salinity are predominantly observed in the western and central North Pacific on the 25.0 and 26.0σ_θ isopycnal surfaces (Fig. 4a–b, d–e). Conversely, positive trends in temperature and salinity are primarily distributed in the northeastern and/or eastern side of the North Pacific along the geostrophic streamlines (Fig. 4a–b, d–e). These results mean that the waters subducted in the frontal region with reduced temperature and salinity originate primarily in the northeastern North Pacific and

https://doi.org/10.5194/egusphere-2025-2746
Preprint. Discussion started: 28 July 2025

are transported south along geostrophic currents (Figs 4a–b, d–e). There are exceptional areas with warmer and saline waters in the northeast North Pacific (170–130°W, 40–60°N). The exceptional waters affect waters that sink near the Alaska gyre and transport outside the subtropical gyre, and along the California coast.

As for the water in the density range of 26.8σ_θ (Fig. 4 g-h), it exhibits large positive trends in potential temperature and salinity along the Kuril Islands and moderate positive trends on the eastern side of the North Pacific, respectively. Water within this density range (26.8σ_θ) is not directly ventilated but is formed through diapycnal mixing processes [Nakamura et al., 2000a, b; Nakamura and Awaji, 2003; You, 2003; Yasuda, 2004] or double diffusion like a salt finger [You, 2003]. Therefore, the positive trends in the North Pacific likely reflect influences from the oxygen change in the upper layer of 26.8σ_θ (Fig. 4d–e and g–h).

The numerical simulation by Ogata and Nonaka [2020] suggested a meridional northward shift of the outcrop line in the North Pacific due to recent climate changes. Similar northward meridional shifts of the front contour lines at 25.0 and 26.0σ_θ are evident in the current data (Fig. 5). These shifts in outcrop densities are therefore attributed to global warming and can explain the observed negative trends, as less saline water from the subarctic region of the North Pacific is subducted and subsequently transported southward via the subtropical circulation. The positive trends in temperature and salinity occurring in the Alaska region [160–130°W, 30–60°N] (Fig. 4a–b and d–e) may also be attributed to the direct influence of global warming. The 26.0σ_θ fronts shift horizontally rather than vertically between 2004 and 2024, therefore (Fig. 5). Therefore, it should be directly affected by the warming and salinity decrease due to global warming, rather than by the water level-directed spreading of the water temperature-salinity distribution.

3.3.2 Dissolved oxygen

The linear trends in dissolved oxygen on the isopycnal surfaces at 25.0, 26.0, and 26.8σ_θ exhibit predominantly negative trends across the North Pacific (Fig. 4c, f, i), but the spatial distributions of

https://doi.org/10.5194/egusphere-2025-2746
Preprint. Discussion started: 28 July 2025

these trends are not uniform. Large negative trends are concentrated in the northeastern and eastern regions, gradually decreasing toward the west (Fig. 4q, f, and i). However, there are exceptions, particularly in the tropical regions, with notable positive trends observed in the western tropical areas on the 26.0 and 26.8σ_θ isopycnal surfaces.

The change of oxygen was decomposed with the same method of Sasano et al. [2004]. The processes and derivation underlying the equations (Eqs. 1, 2) for the change of dissolved oxygen are as follows. We tried to calculate each factor below and discussed the contributing factors for the dissolved oxygen.

$$\frac{\partial O_2}{\partial t} = \left(\frac{\partial O_2}{\partial z}\frac{\partial z}{\partial t}\right) + \left(\frac{\partial O_2^{sat}}{\partial t}\right)_{net} - \left(\frac{\partial (AOU)}{\partial t}\right)_{net}, \quad (1)$$

and consequently, they proposed the following equation:

$$\frac{\partial O_2}{\partial t} = \left(\frac{\partial O_2}{\partial z}\frac{\partial z}{\partial t}\right) + \left(\frac{\partial O_2^{sat}}{\partial t} - \frac{\partial O_2^{sat}}{\partial z}\frac{\partial z}{\partial t}\right) + \left(-\frac{\partial (AOU)}{\partial t} + \frac{\partial (AOU)}{\partial z}\frac{\partial z}{\partial t}\right). \quad (2)$$

(i) (ii). (iii). (iv) (v) (vi)

$\partial O_2/\partial t$ ($X = O_2$, O_2^{sat}, AOU (Apparent Oxygen Utilization)) and $\partial z/\partial t$ denote the temporal rate of change in the depth of the isopycanl horizon (z), while $\partial X/\partial z$ indicates the vertical gradient of the variable X at that horizon., The latter was averaged over the past 20 years in this analysis. The term ($\partial X/\partial t$)$_{net}$ represents the net change in a variable X. By applying Eq. (2) to the time-series data of the reconstructed O_2 data estimated from the linear regression analysis, the rate of O_2 change on each isopycnal horizon (i) was attributed to various factors: (ii) the apparent effect of the deepening of isopycnal horizon due to warming/freshening; (iii) the effect of O_2^{sat} change due to temperature/salinity changes; (iv) the effect of the deepening/shallowness of isopycnal horizons with temperature/salinity changes; (v) the changes in AOU resulting from factors such as disequilibrium with atmosphere, biological activities with lateral advection and/or circulation (the elapsed time after the water lost contact with the atmosphere); (vi) the effect of deepening/shallowing of AOU changes unrelated to O_2^{sat}.

https://doi.org/10.5194/egusphere-2025-2746
Preprint. Discussion started: 28 July 2025

Figure 6 shows the horizontal distributions of the magnitude of each factor contributing to the rate of O_2 change on 25.0σ_θ, 26.0σ_θ and 26.8σ_θ surfaces. The results showed that the prominent O_2 declines (Fig. 5c, f, i) are driven by multiple contributing negative and positive factors. The dominant factors vary by latitude. Around Alaska Gyre in higher latitudes (170–130°W, 40–60°N), the primary contributors to O_2 decline are the deepening of isopycnal horizons (ii) and the shallowing of AOU changes (vi) (Fig. 6f, j, k, o). The effect of O_2^{sat} change due to temperature/salinity (iii) and the AOU changes (v) are affected oppositely at that time. The negative trends in the Bering Sea (150°E–170°W, 50–60°N) (Figs. 4o) can be judged to be mainly affected by the AOU changes (v) (Fig. 6n).

In contrast, the O_2 decline in the subtropical and mid-latitudes (10–40°N) is largely driven by AOU changes (v) (Fig. 6d, i, and n). The relative weakening of the total O_2 decline in the western North Pacific (Fig. 4c, f, i) is influenced by positive O_2 changes (Fig. 6f and k). Such positive trends are driven by O_2^{sat} changes due to temperature and salinity (Fig. 6b), and/or the deepening of AOU (Fig. 6j and o) (Fig. 7b and c).

Slightly in the mid-ocean between 170°E and 160°W, the positive trend pattern shows a negative trend, but in the North Pacific Ocean between 30°N and 50°N, there is a pronounced positive trend continuously extending from east to west (Fig. 6i and n). This phenomenon may be related to the northward meridional shift of the fronts between the subtropical and subarctic regions due to global warming [Ogata and Nonaka, 2020]. With deeper winter convection, more nutrients are introduced into the surface layer, potentially enhancing biological activity and leading to an increase in AOU. One area of NPIW formation near the Kuril Islands exhibits negative trends in factor (iii) (Fig. 6l). This result suggests weaker vertical mixing during the observational period, likely related to enhanced surface-layer stratification. Supporting this, the current data show positive trends in both temperature and salinity in this region (Fig. 4g–h).

https://doi.org/10.5194/egusphere-2025-2746
Preprint. Discussion started: 28 July 2025

The increases in O_2 are particularly prominent in the western tropical area (0–10°N) at the density range of 26.8–27.2 σ_θ (Fig. 2c and f; Fig. 3c and f; Fig. 4c, f, and i). This area overlaps with the OML. A similar tendency is reported by Sasano et al. [2014] and Takatani et al. [2012]. In this area, it has been observed that the North Equatorial Current (NEC) and the North Equatorial Counter Current (NECC) have migrated southward and strengthened in the western North Pacific between 1993 and 2009 [Qui and Chen, 2012]. The westward penetration of the OML is slow, occurring between two eastward-extending tongues of high O_2 water originating from the western boundary [Reid, 1997]. Sasano et al. [2014] explained this O_2 increase from the southward migration and strengthening of the NEC and NECC: i.e. the westward and northward expansion of the OML would be suppressed, consequently enhancing O_2 concentrations in the western tropical Pacific, most notably in the northern part of the OML near the NEC. Qui and Chen's study used observational data from 1993 to 2009 and reported this physical phenomenon, but this physical phenomenon likely continues due to its association with recent global warming. In fact, the NEC and NECC flow westward between 5° and 15°N, and we detected that the depth of the isopycnal surface became shallower during the observational period in the boundary between the subtropical gyre and the tropical region (Fig. 7). These results therefore further support the previous argument (Fig. 4b, e, and h).

4. Conclusion

The oxygen variabilities in the North Pacific include the influences of global warming and climate variabilities. We focused on the linear trends for the past 20 years with the four-dimensional grided [O_2] product [GOBAI-O_2] in the North Pacific, based on the historical hydrographic cruise data and the profiling float data, with the Artificial Intelligence technique [Sharp et al. 2023]. This study uses GOBAI-O_2 data to examine linear trends in potential water temperature, salinity, and dissolved oxygen in the North Pacific over the past 20 years (2004–2023) and the mechanisms behind these trends. The linear trends in potential water temperature, salinity, and dissolved oxygen are consistent with findings

https://doi.org/10.5194/egusphere-2025-2746
Preprint. Discussion started: 28 July 2025

from previous studies and how they change spatially along 137°E and 165°E (Figs. 2 and 3). In addition, we found the horizontal trend mapping over the North Pacific area along the isopycnals (Fig. 4). In particular, the oxygen data, which were less abundant than those for water temperature and salinity and had previously been known only piecemeal, showed that along with the overall decrease in oxygen concentrations, there were also areal areas where there was a local trend of increasing oxygen concentrations (Fig. 4). From dissolved O_2 decomposed analysis, we further confirmed possible sources of O_2 trend in each isopycnal (Fig. 6).

The detected linear trends showed a similar tendency in temperature, salinity, and dissolved oxygen in the previous historical studies [Takatani et al. 2012; Sasano et al. 2014; Ogata and Nonaka, 2020]. Since the GOBAI- O_2 data are gridded, the tendencies were shown to be smoothly connected spreading horizontally vertically to the west and east. Of course, we see some artificial unnatural spreading (e.g. 170–130°W, 0–20°N), especially in dissolved oxygen (Fig. 1q–s; Fig. 4i).

Uncertainty estimates (Fig. A) clearly show some spots and depths having the large values, sometimes more than 40 μmol/kg, but normally the uncertainty estimates within 10 μmol/kg in the North Pacific. This would occur due to limited observational data and high background variability [Sharp et al. 2023]. The results of this analysis, however, showed that the trends are connected horizontally, and we could link their trends to well-known physical mechanisms in the North Pacific. The GOBAI-O_2 dataset is, therefore expected to provide a better understanding of other oceanic biogeochemical processes and physical phenomena from an areal perspective.

PDO [Stramma et al. 2020] and North Pacific Gyre Oscillation (NPGO) [Stramma et al. 2020] decadal variability (Pacific Decadal Oscillation) [Pozo Buil and Di Lorenzo, 2017], are known as the low-frequency climate variability in the North Pacific. It has not been difficult to discuss the spatial distribution and temporal changes of the low-frequent climate variability in the four-dimensional area, but the GOBAI-O_2 data are produced in a monthly dataset and seemingly one of the useful tools to explore such target research focusing on the influences of dissolved oxygen in terms of the expected physical low-frequency climate mechanism. We leave this topic in future study.

https://doi.org/10.5194/egusphere-2025-2746
Preprint. Discussion started: 28 July 2025

Data availability:

GOBAI-O_2 data is available at https://www.ncei.noaa.gov/access/metadata/landing-page/bin/iso?id=gov.noaa.nodc:0259304. Temperature and salinity are from Roemmich and Gilson (2009) Argo climatology (https://sio-argo.ucsd.edu/RG_Climatology.html).

Acknowledgements:

This work was supported by the Institute for Basic Science (IBS), Republic of Korea, under IBS-R028-D1. Jonathan D. Sharp and the reviewers are acknowledged for providing comments that prompted significant improvements to this manuscript.

Author contributions:

MI designed the study, and wrote the initial manuscript draft, and produced all figures. All authors contributed to checking and improving the manuscript.

Financial support:

This research has been supported by the Institute for Basic Science (grant no. IBS-R028-D1) and the Japan Society for the Promotion of Science (JSPS) through a Grant-in-Aid for Scientific Research JP22H00176.

Figure captions:

https://doi.org/10.5194/egusphere-2025-2746
Preprint. Discussion started: 28 July 2025

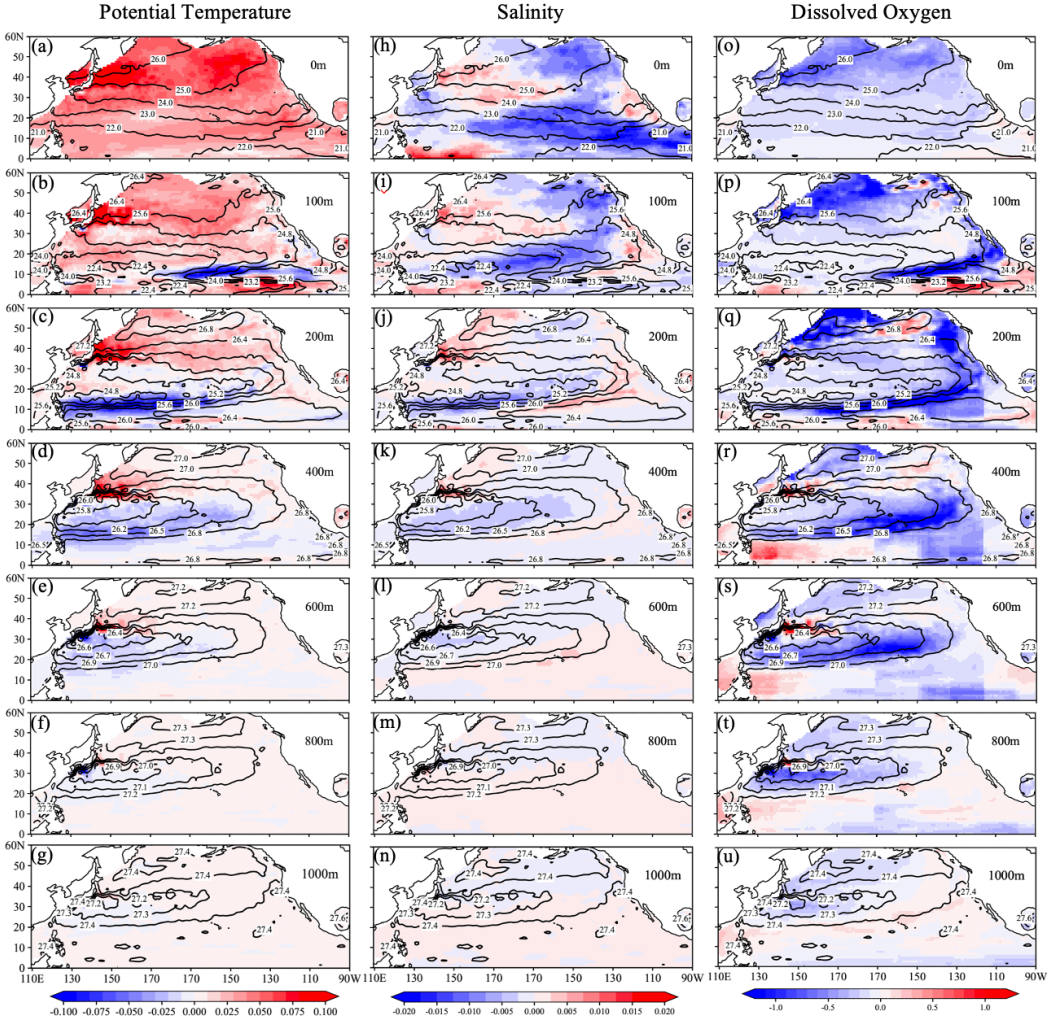

Figure 1 Horizontal distributions of linear trends in (a–g) potential temperature, (h–n) salinity, and (o–u) dissolved oxygen during the observational period at depths of 0, 100, 200, 400, 600, 800, and 1000 m, respectively. Contours denote potential density at each depth.

https://doi.org/10.5194/egusphere-2025-2746
Preprint. Discussion started: 28 July 2025

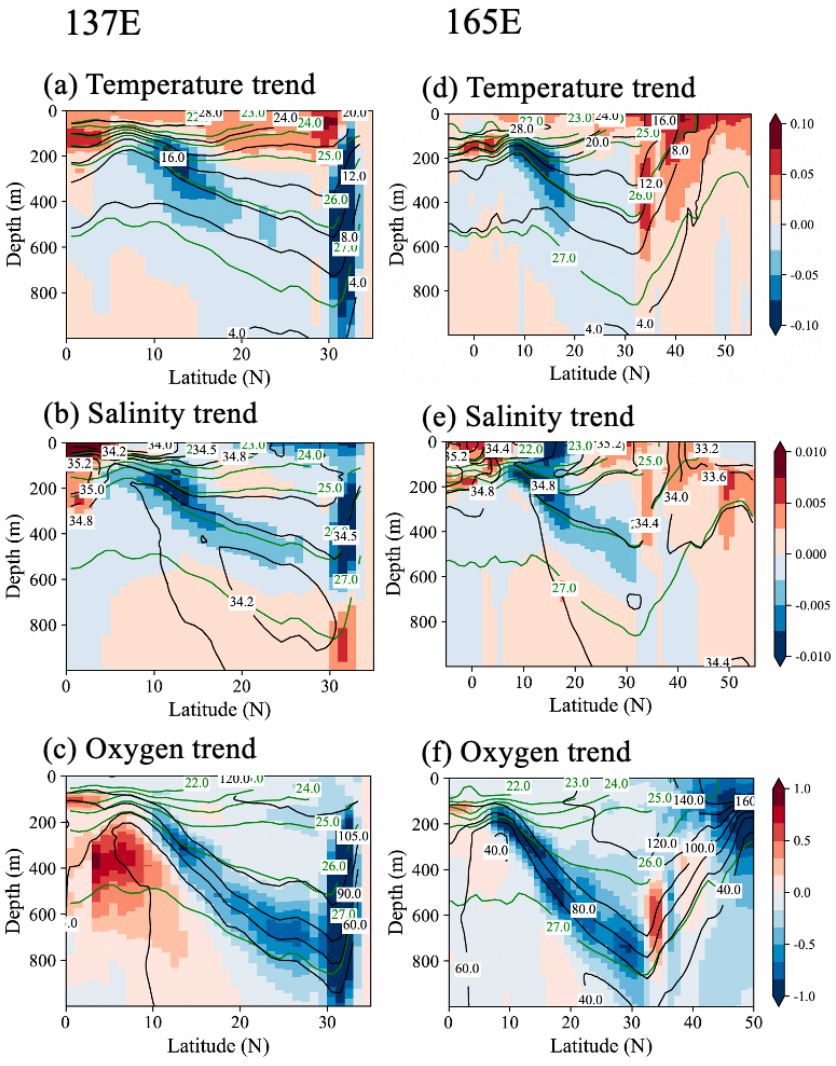

Figure 2 Vertical sections of linear trends in potential temperature (a, d), salinity (b, e), and dissolved oxygen (c, f) along the 137°E and 165°E lines, respectively. Black contour lines represent the average potential temperature (a, d), salinity (b, e), and dissolved oxygen (c, f) during the period 2004–2023. Green contour lines indicate the average potential density (a–f).

https://doi.org/10.5194/egusphere-2025-2746
Preprint. Discussion started: 28 July 2025

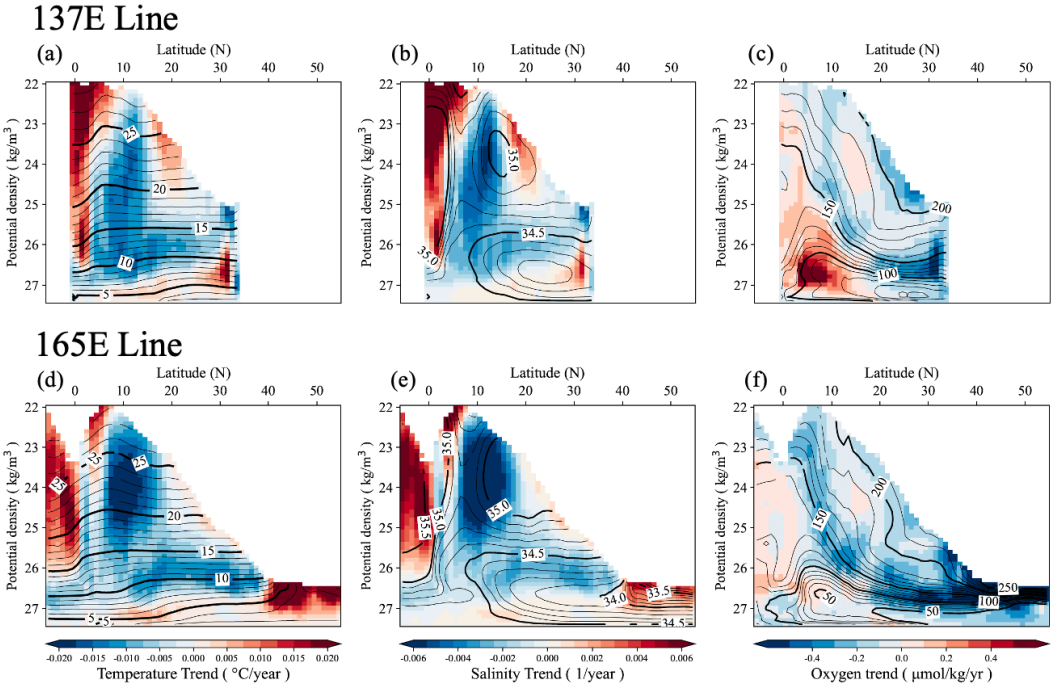

Figure 3 Linear trends in (a) potential temperature, (b) salinity, and (c) dissolved O_2 on each isopycnal horizon at intervals of $0.1\sigma_\theta$, calculated at every 1.0 deg of latitude in 137 °E and 165 °E lines, respectively. Contour lines represent the mean values during the target observation periods, plotted at intervals of $0.1\sigma_\theta$ for each 1 deg of latitude.

https://doi.org/10.5194/egusphere-2025-2746
Preprint. Discussion started: 28 July 2025

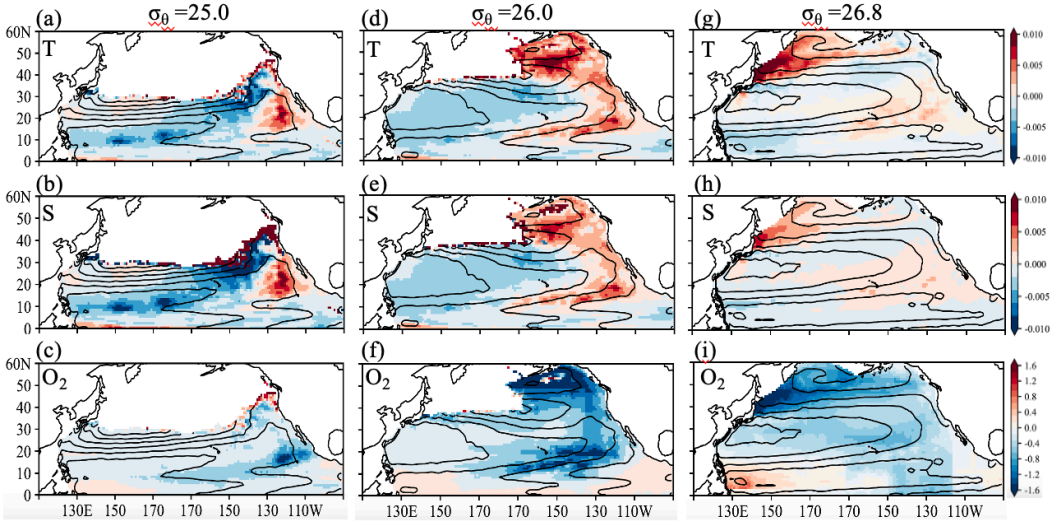

Figure 4 Linear trends in (a) potential temperature, (b) salinity, and (c) dissolved O_2 on each isopycnal horizon at 25.0, 26.0, and 26.8σ_θ. Contour lines represent geostrophic flow streamlines on 26.0 and 26.8σ_θ surface, relative to 2000 dbar.

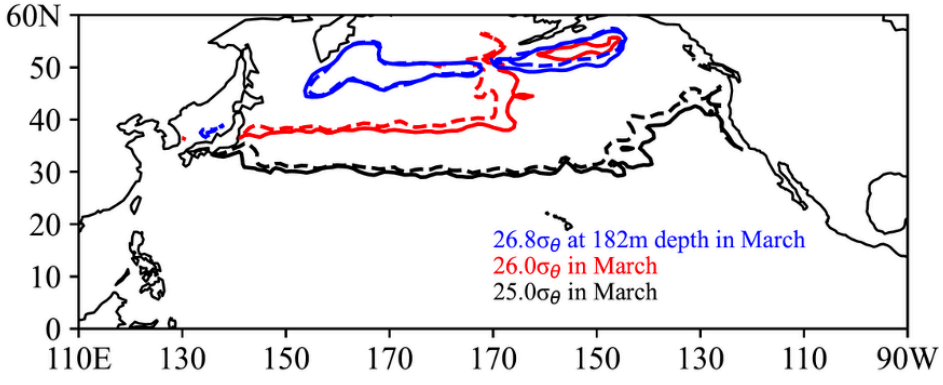

Figure 5 Density contours of 25.0σ_θ (black), 26.0σ_θ (red), and 26.8σ_θ (blue). Solid lines indicate the average density contours for March 2004–2009, while dashed lines represent 2019–2023.

https://doi.org/10.5194/egusphere-2025-2746
Preprint. Discussion started: 28 July 2025

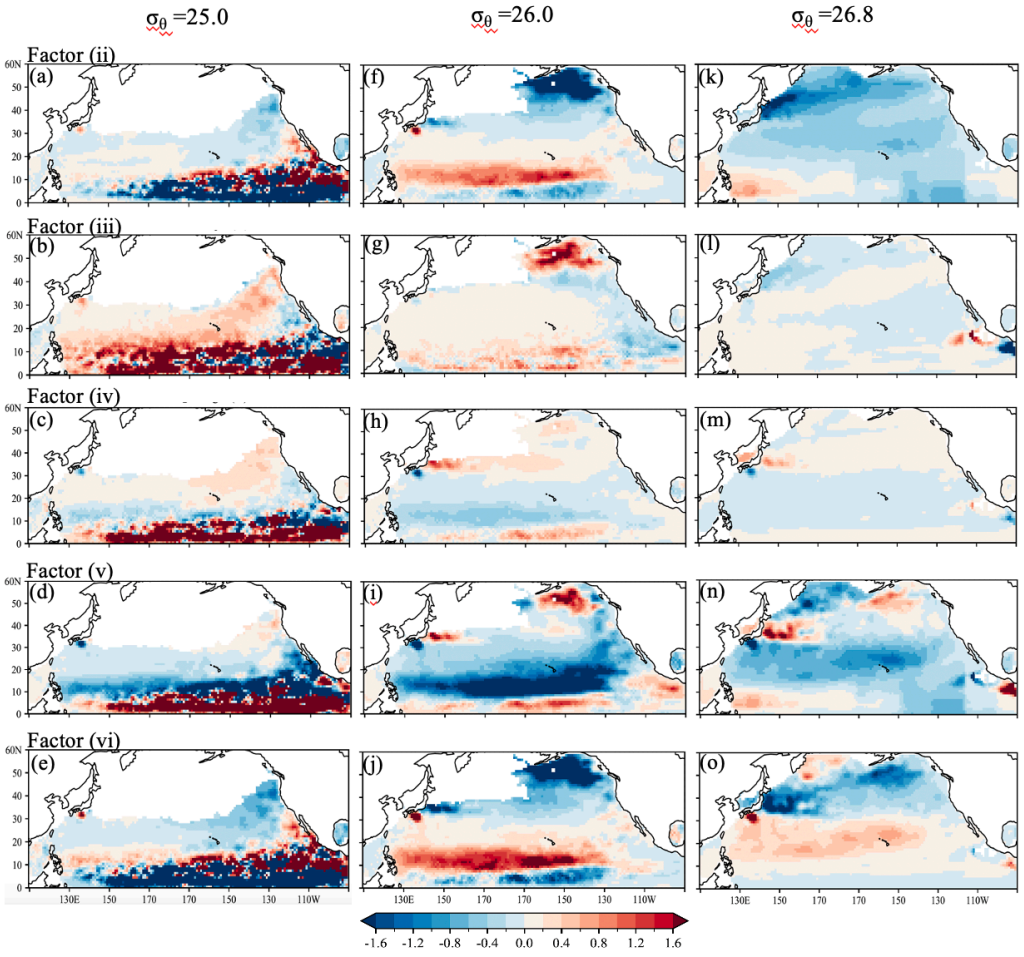

Figure 6 Horizontal distributions of the magnitude of each factor contributing to the rate of O_2 change on 25.0, 26.0, and 26.8 σ_θ in Eq. (1). The rate of O_2 change on each isopycnal horizon is attributed to these factors: (ii) the apparent effect of the deepening of the isopycnal horizon due to warming/ refreshing, (iii) the effect of O_2^{sat} change due to temperature/salinity changes, (iv) the effect of the deepening/shallowness of isopycnal horizons with temperature/salinity changes, (v) the changes in AOU resulting from factors such as disequilibrium with atmosphere, biological activities with lateral advection and/or circulation, (vi) the effect of deepening/shallowing of AOU changes unrelated to O_2^{sat}. This analysis was calculated with the reconstructed O_2 data estimated from the linear regression analysis.

https://doi.org/10.5194/egusphere-2025-2746
Preprint. Discussion started: 28 July 2025

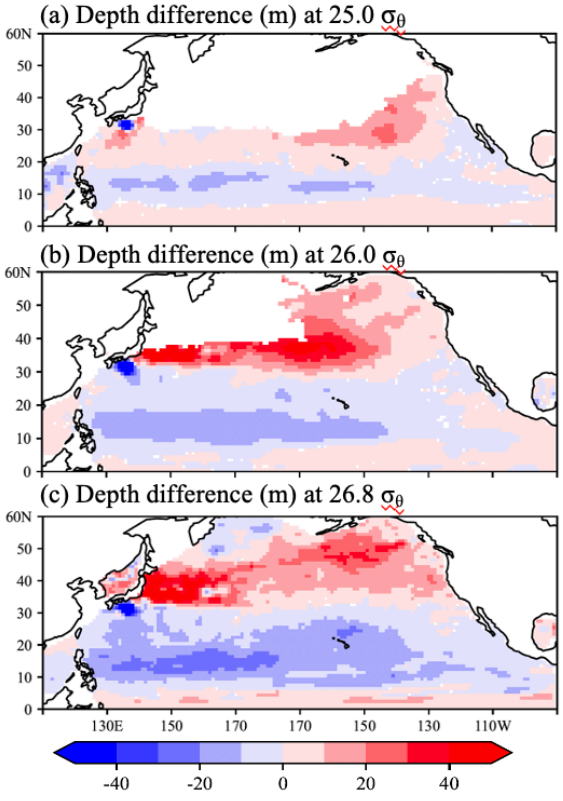

Figure 7 Depth difference (m) between the 5-year averaged data in March, 2004–2009 and 2018–2023 at 25.0, 26.0, and 26.8σ_θ. The reconstructed O_2 data estimated from the linear regression analysis were used in this calculation. Positive and negative values indicate the deepening and shallowing, respectively, from the depth of each density in 2018– 2023.

https://doi.org/10.5194/egusphere-2025-2746
Preprint. Discussion started: 28 July 2025

References:

Alkire, M. B., D'Asaro, E., Lee, C., Jane Perry, M., Gray, A., Cetinić, I., et al. (2012). Estimates of net community production and export using high-resolution, Lagrangian measurements of O2, NO3−, and POC through the evolution of a spring diatom bloom in the North Atlantic. *Deep Sea Research Part I: Oceanographic Research Papers*, *64*, 157–174. https://doi.org/10.1016/j.dsr.2012.01.012

Berman-Frank, I., Lundgren, P., & Falkowski, P. (2003). Nitrogen fixation and photosynthetic oxygen evolution in cyanobacteria. *Research in Microbiology*, *154*(3), 157–164. https://doi.org/10.1016/S0923-2508(03)00029-9

Bopp, L., Resplandy, L., Orr, J. C., Doney, S. C., Dunne, J. P., Gehlen, M., et al. (2013). Multiple stressors of ocean ecosystems in the 21st century: projections with CMIP5 models. *Biogeosciences*, *10*(10), 6225–6245. https://doi.org/10.5194/bg-10-6225-2013

Breiman, L. (2001). Random Forests. *Machine Learning*, *45*(1), 5–32. https://doi.org/10.1023/A:1010933404324

Breitburg, D., Levin, L. A., Oschlies, A., Grégoire, M., Chavez, F. P., Conley, D. J., et al. (2018). Declining oxygen in the global ocean and coastal waters. *Science*, *359*(6371), eaam7240. https://doi.org/10.1126/science.aam7240

Bushinsky, S. M., Emerson, S. R., Riser, S. C., & Swift, D. D. (2016). Accurate oxygen measurements on modified Argo floats using in situ air calibrations. *Limnology and Oceanography: Methods*, *14*(8), 491–505. https://doi.org/10.1002/lom3.10107

https://doi.org/10.5194/egusphere-2025-2746
Preprint. Discussion started: 28 July 2025

Claustre, H., Johnson, K. S., & Takeshita, Y. (2020). Observing the Global Ocean with Biogeochemical-Argo. *Annual Review of Marine Science*, *12*(Volume 12, 2020), 23–48. https://doi.org/10.1146/annurev-marine-010419-010956

D'Asaro, E. A., & McNeil, C. (2013). Calibration and Stability of Oxygen Sensors on Autonomous Floats. https://doi.org/10.1175/JTECH-D-12-00222.1

Drucker, R., & Riser, S. C. (2016). In situ phase-domain calibration of oxygen Optodes on profiling floats. *Methods in Oceanography*, *17*, 296–318. https://doi.org/10.1016/j.mio.2016.09.007

Estapa, M. L., Feen, M. L., & Breves, E. (2019). Direct Observations of Biological Carbon Export From Profiling Floats in the Subtropical North Atlantic. *Global Biogeochemical Cycles*, *33*(3), 282–300. https://doi.org/10.1029/2018GB006098

Giglio, D., Lyubchich, V., & Mazloff, M. R. (2018). Estimating Oxygen in the Southern Ocean Using Argo Temperature and Salinity. *Journal of Geophysical Research: Oceans*, *123*(6), 4280–4297. https://doi.org/10.1029/2017JC013404

Helm, K. P., Bindoff, N. L., & Church, J. A. (2011). Observed decreases in oxygen content of the global ocean. *Geophysical Research Letters*, *38*(23). https://doi.org/10.1029/2011GL049513

Information (NCEI), N. C. for E. (n.d.). GOBAI-O2: A Global Gridded Monthly Dataset of Ocean Interior Dissolved Oxygen Concentrations Based on Shipboard and Autonomous Observations (NCEI Accession 0259304). Retrieved January 14, 2025, from https://www.ncei.noaa.gov/access/metadata/landing-page/bin/iso?id=gov.noaa.nodc:0259304

https://doi.org/10.5194/egusphere-2025-2746
Preprint. Discussion started: 28 July 2025

Ito, T., Minobe, S., Long, M. C., & Deutsch, C. (2017). Upper ocean O2 trends: 1958–2015. *Geophysical Research Letters*, *44*(9), 4214–4223. https://doi.org/10.1002/2017GL073613

Johnson, K. S., & Bif, M. B. (2021). Constraint on net primary productivity of the global ocean by Argo oxygen measurements. *Nature Geoscience*, *14*(10), 769–774. https://doi.org/10.1038/s41561-021-00807-z

Johnson, K. S., Plant, J. N., Riser, S. C., & Gilbert, D. (2015). Air Oxygen Calibration of Oxygen Optodes on a Profiling Float Array. https://doi.org/10.1175/JTECH-D-15-0101.1

Johnson, K. S., Plant, J. N., Coletti, L. J., Jannasch, H. W., Sakamoto, C. M., Riser, S. C., et al. (2017). Biogeochemical sensor performance in the SOCCOM profiling float array. *Journal of Geophysical Research: Oceans*, *122*(8), 6416–6436. https://doi.org/10.1002/2017JC012838

Keeling, R. F., Körtzinger, A., & Gruber, N. (2010). Ocean Deoxygenation in a Warming World. *Annual Review of Marine Science*, *2*(Volume 2, 2010), 199–229. https://doi.org/10.1146/annurev.marine.010908.163855

Kwiatkowski, L., Torres, O., Bopp, L., Aumont, O., Chamberlain, M., Christian, J. R., et al. (2020). Twenty-first century ocean warming, acidification, deoxygenation, and upper-ocean nutrient and primary production decline from CMIP6 model projections. *Biogeosciences*, *17*(13), 3439–3470. https://doi.org/10.5194/bg-17-3439-2020

https://doi.org/10.5194/egusphere-2025-2746
Preprint. Discussion started: 28 July 2025

517 Lauvset, S. K., Lange, N., Tanhua, T., Bittig, H. C., Olsen, A., Kozyr, A., et al. (2022).
518 GLODAPv2.2022: the latest version of the global interior ocean biogeochemical data product. *Earth*
519 *System Science Data*, *14*(12), 5543–5572. https://doi.org/10.5194/essd-14-5543-2022
520 Li, C., Huang, Jianping, Ding, L., Liu, X., Yu, H., Huang, Jiping, 2020. Increasing Escape of Oxygen
521 From Oceans Under Climate Change. Geophysical Research Letters 47, e2019GL086345.
522 https://doi.org/10.1029/2019GL086345
523 Limburg, K. E., Breitburg, D., Swaney, D. P., & Jacinto, G. (2020). Ocean Deoxygenation: A Primer.
524 *One Earth*, *2*(1), 24–29. https://doi.org/10.1016/j.oneear.2020.01.001
525 Maurer, T. L., Plant, J. N., & Johnson, K. S. (2021). Delayed-Mode Quality Control of Oxygen, Nitrate,
526 and pH Data on SOCCOM Biogeochemical Profiling Floats. *Frontiers in Marine Science*, *8*.
527 https://doi.org/10.3389/fmars.2021.683207
528 Nakamura, T., & Awaji, T. (2004). Tidally induced diapycnal mixing in the Kuril Straits and its role
529 in water transformation and transport: A three-dimensional nonhydrostatic model experiment. *Journal*
530 *of Geophysical Research: Oceans*, *109*(C9). https://doi.org/10.1029/2003JC001850
531 Nakamura, T., Awaji, T., Hatayama, T., Akitomo, K., Takizawa, T., Kono, T., et al. (2000). The
532 Generation of Large-Amplitude Unsteady Lee Waves by Subinertial K1 Tidal Flow: A Possible
533 Vertical Mixing Mechanism in the Kuril Straits. Retrieved from
534 https://journals.ametsoc.org/view/journals/phoc/30/7/1520-
535 0485_2000_030_1601_tgolau_2.0.co_2.xml

https://doi.org/10.5194/egusphere-2025-2746
Preprint. Discussion started: 28 July 2025

536 Nakamura, T., Awaji, T., Hatayama, T., Akitomo, K., & Takizawa, T. (2000). Tidal Exchange through
537 the Kuril Straits. Retrieved from https://journals.ametsoc.org/view/journals/phoc/30/7/1520-
538 0485_2000_030_1622_tettks_2.0.co_2.xml
539 Nicholson, D. P., & Feen, M. L. (2017). Air calibration of an oxygen optode on an underwater glider.
540 *Limnology and Oceanography: Methods*, *15*(5), 495–502. https://doi.org/10.1002/lom3.10177
541 Ogata, T., & Nonaka, M. (2020). Mechanisms of Long-Term Variability and Recent Trend of Salinity
542 Along 137°E. *Journal of Geophysical Research: Oceans*, *125*(2), e2019JC015290.
543 https://doi.org/10.1029/2019JC015290
544 Oka, E., Katsura, S., Inoue, H., Kojima, A., Kitamoto, M., Nakano, T., & Suga, T. (2017). Long-term
545 change and variation of salinity in the western North Pacific subtropical gyre revealed by 50-year long
546 observations along 137°E. *Journal of Oceanography*, *73*(4), 479–490. https://doi.org/10.1007/s10872-
547 017-0416-2
548 Pörtner, H. O., & Farrell, A. P. (2008). Physiology and Climate Change. *Science*, *322*(5902), 690–692.
549 https://doi.org/10.1126/science.1163156
550 Pozo Buil, M., & Di Lorenzo, E. (2017). Decadal dynamics and predictability of oxygen and
551 subsurface tracers in the California Current System. *Geophysical Research Letters*, *44*(9), 4204–4213.
552 https://doi.org/10.1002/2017GL072931
553 Qiu, B., & Chen, S. (2012). Multidecadal Sea Level and Gyre Circulation Variability in the
554 Northwestern Tropical Pacific Ocean. https://doi.org/10.1175/JPO-D-11-061.1

https://doi.org/10.5194/egusphere-2025-2746
Preprint. Discussion started: 28 July 2025

555 Reid, J. L. (1997). On the total geostrophic circulation of the pacific ocean: flow patterns, tracers, and
556 transports. *Progress in Oceanography*, *39*(4), 263–352. https://doi.org/10.1016/S0079-
557 6611(97)00012-8

558 Roemmich, D., & Gilson, J. (2009). The 2004–2008 mean and annual cycle of temperature, salinity,
559 and steric height in the global ocean from the Argo Program. *Progress in Oceanography*, *82*(2), 81–
560 100. https://doi.org/10.1016/j.pocean.2009.03.004

561 Sampaio, E., Santos, C., Rosa, I. C., Ferreira, V., Pörtner, H.-O., Duarte, C. M., et al. (2021). Impacts
562 of hypoxic events surpass those of future ocean warming and acidification. *Nature Ecology &*
563 *Evolution*, *5*(3), 311–321. https://doi.org/10.1038/s41559-020-01370-3

564 Sasano, D., Takatani, Y., Kosugi, N., Nakano, T., Midorikawa, T., & Ishii, M. (2018). Decline and
565 Bidecadal Oscillations of Dissolved Oxygen in the Oyashio Region and Their Propagation to the
566 Western North Pacific. *Global Biogeochemical Cycles*, *32*(6), 909–931.
567 https://doi.org/10.1029/2017GB005876

568 Schmidtko, S., Stramma, L., & Visbeck, M. (2017). Decline in global oceanic oxygen content during
569 the past five decades. *Nature*, *542*(7641), 335–339. https://doi.org/10.1038/nature21399

570 Sharp, J. D., Fassbender, A. J., Carter, B. R., Johnson, G. C., Schultz, C., & Dunne, J. P. (2023a).
571 GOBAI-O_2: temporally and spatially resolved fields of ocean interior dissolved oxygen over nearly 2
572 decades. *Earth System Science Data*, *15*(10), 4481–4518. https://doi.org/10.5194/essd-15-4481-2023

https://doi.org/10.5194/egusphere-2025-2746
Preprint. Discussion started: 28 July 2025

573 Sharp, J. D., Fassbender, A. J., Carter, B. R., Johnson, G. C., Schultz, C., & Dunne, J. P. (2023b).
574 GOBAI-O_2: temporally and spatially resolved fields of ocean interior dissolved oxygen over nearly 2
575 decades. *Earth System Science Data*, *15*(10), 4481–4518. https://doi.org/10.5194/essd-15-4481-2023
576 Stramma, L., & Schmidtko, S. (2021). Tropical deoxygenation sites revisited to investigate oxygen
577 and nutrient trends. *Ocean Science*, *17*(3), 833–847. https://doi.org/10.5194/os-17-833-2021
578 Stramma, L., Schmidtko, S., Bograd, S. J., Ono, T., Ross, T., Sasano, D., & Whitney, F. A. (2020).
579 Trends and decadal oscillations of oxygen and nutrients at 50 to 300 m depth in the equatorial
580 and North Pacific. *Biogeosciences*, *17*(3), 813–831. https://doi.org/10.5194/bg-17-813-2020
581 Suga, T., Takei, Y., & Hanawa, K. (1997). Thermostad Distribution in the North Pacific Subtropical
582 Gyre: The Central Mode Water and the Subtropical Mode Water. Retrieved from
583 https://journals.ametsoc.org/view/journals/phoc/27/1/1520-
584 0485_1997_027_0140_tditnp_2.0.co_2.xml
585 Suga, T., Motoki, K., Aoki, Y., & Macdonald, A. M. (2004). The North Pacific Climatology of Winter
586 Mixed Layer and Mode Waters. Retrieved from
587 https://journals.ametsoc.org/view/journals/phoc/34/1/1520-
588 0485_2004_034_0003_tnpcow_2.0.co_2.xml
589 Takatani, Y., Sasano, D., Nakano, T., Midorikawa, T., & Ishii, M. (2012). Decrease of dissolved
590 oxygen after the mid-1980s in the western North Pacific subtropical gyre along the 137°E repeat
591 section. *Global Biogeochemical Cycles*, *26*(2). https://doi.org/10.1029/2011GB004227

https://doi.org/10.5194/egusphere-2025-2746
Preprint. Discussion started: 28 July 2025

592 Udaya Bhaskar, T. V. S., Sarma, V. V. S. S., & Pavan Kumar, J. (2021). Potential Mechanisms
593 Responsible for Spatial Variability in Intensity and Thickness of Oxygen Minimum Zone in the Bay
594 of Bengal. *Journal of Geophysical Research: Biogeosciences*, *126*(6), e2021JG006341.
595 https://doi.org/10.1029/2021JG006341

596 Winkler, L. W. (1888). Die Bestimmung des im Wasser gelösten Sauerstoffes. *Berichte Der Deutschen*
597 *Chemischen Gesellschaft*, *21*(2), 2843–2854. https://doi.org/10.1002/cber.188802102122

598 Wolf, M. K., Hamme, R. C., Gilbert, D., Yashayaev, I., & Thierry, V. (2018). Oxygen Saturation
599 Surrounding Deep Water Formation Events in the Labrador Sea From Argo-O2 Data. *Global*
600 *Biogeochemical Cycles*, *32*(4), 635–653. https://doi.org/10.1002/2017GB005829

601 Yasuda, I. (2004). North Pacific Intermediate Water: Progress in SAGE (SubArctic Gyre Experiment)
602 and Related Projects. *Journal of Oceanography*, *60*(2), 385–395.
603 https://doi.org/10.1023/B:JOCE.0000038344.25081.42

604 You, Y. (2003). The pathway and circulation of North Pacific Intermediate Water. *Geophysical*
605 *Research Letters*, *30*(24). https://doi.org/10.1029/2003GL018561

606
607
608
609

610